Frontiers in Bioscience Landmark

Front. Biosci. (Landmark Ed) **2026**; 31(9): 53784
https://doi.org/10.31083/FBL53784

Original Research

Multi-Organ Metatranscriptomics Establishes Organ-Specific Functional Baselines in the Crested Ibis (*Nipponia nippon*)

Guoqiang Qiu[1,†], Jinshi Ran[2,3,†], Jian Shi[1], Liying Yuan[1], Wenwen Dai[1], Jichen Jin[2,3], Pengqi Zhang[2,3], Xiaojun Wang[4], Xinyue Chen[4], Chen Li[4,*], Yongmei Xi[2,3,*]

[1]Deqing County Ecological Forestry Comprehensive Service Center, Deqing County Bureau of Natural Resources and Planning, 313200 Deqing, Zhejiang, China
[2]Institute of Genetics, Zhejiang University International School of Medicine, 310058 Hangzhou, Zhejiang, China
[3]Center for Genetic Medicine, The Fourth Affiliated Hospital, Zhejiang University School of Medicine, 322000 Yiwu, Zhejiang, China
[4]Department of Human Genetics, and Women's Hospital, Zhejiang University School of Medicine, 310058 Hangzhou, Zhejiang, China
*Correspondence: chenli2012@zju.edu.cn (Chen Li); xyyongm@zju.edu.cn (Yongmei Xi)
[†]These authors contributed equally.
Academic Editor: Graham Pawelec
Submitted: 12 November 2025 Revised: 12 May 2026 Accepted: 27 July 2026 Published: 18 September 2026

Abstract

Background: The crested ibis (*Nipponia nippon*) is an iconic East Asian species on the International Union for Conservation of Nature's (IUCN) Red List, with recurrent stress-related sudden death reported in captivity and in the wild. However, the mechanisms underlying stress responses remain poorly characterized. **Methods:** Using opportunistic post-mortem samples, we generated, to our knowledge, the first organ-resolved metatranscriptomic reference dataset for this species in a stress-associated context. Matched libraries from small intestine, liver, spleen, and lung were sequenced and processed using a unified pipeline; microbial transcriptional activity was quantified following host and rRNA removal and stringent detection criteria, enabling concurrent readouts of community composition and functional gene expression. **Results:** Transcriptional activity was intestine-centric, whereas liver, spleen, and lung harbored low-load communities with limited taxon sharing. The small intestine was dominated by the aquatic-associated *Cetobacterium somerae* (~54.8%), consistent with fish-based feeding, while *Romboutsia* was scarce, suggesting a weak butyrate-producing guild. Functionally, transcripts were enriched for small-molecule metabolism, nucleotide/cofactor turnover, central carbon conversion, and membrane/envelope-associated precursor pathways. Stratified pathway analysis further resolved uneven classified contributions: *Paraclostridium bifermentans* spanned the broadest classified pathway repertoire, *Cetobacterium somerae* contributed more strongly to nucleotide-linked functions, and *Clostridium perfringens* retained a more distinctive inositol-related branch. Antimicrobial resistance (AMR)-linked transcripts in the intestine were dominated by target-site mechanisms (elongation factor Tu (EF-Tu), RNA polymerase β′ subunit (rpoC) and DNA gyrase subunit A (gyrA)) with a low-level ErmQ-associated macrolide–lincosamide–streptogramin (MLS) resistance signature, consistent with background expression of core targets. **Conclusions:** This organ-resolved dataset provides a practical baseline for microbiome, pathogen, and resistance surveillance in captive crested ibis, and a reference for future comparisons among captive, wild, and reintroduced populations. AMR signals are best read as contextual markers rather than phenotypic resistance and can serve as auxiliary sentinels alongside composition and function. Overall, the dataset provides a reusable framework for health assessment and conservation planning.

Keywords: crested ibis (*Nipponia nippon*); metatranscriptomics; organ-resolved microbiome; antimicrobial resistance; conservation biology

1. Introduction

The crested ibis (*Nipponia nippon*) is an emblematic East Asian species and a recognized umbrella species for conservation. Despite population gains from captive breeding and reintroduction in China, Japan, and Korea, maintaining health, managing stress, and conducting disease surveillance remain persistent challenges in captive and semi-wild settings [1,2]. Growing evidence indicates that the microbiome underpins nutrition, mucosal barrier integrity, and immune homeostasis, and via gut–immune–neuroendocrine axes, can modulate behavior and stress responses, with consequences for condition and reproductive success in threatened species [3,4,5].

In birds, acute stressors engage both the hypothalamic–pituitary–adrenal (HPA) axis and the sympathetic–adrenomedullary (SAM) system, elevating corticosterone, via the principal avian glucocorticoid and catecholamines to mobilize energy and prioritize short-term survival [6,7,8]. When activation is frequent or prolonged, accumulated allostatic load can depress mucosal immunity, dysregulate metabolism, and constrain growth and reproduction [9,10]. Microbiome-derived metabolites, including short-chain fatty acids and bile-acid/tryptophan derivatives signal through vagal, immune, and endocrine routes such as FFAR2/3, FXR/TGR5, to shape HPA reactivity and inflammation [11,12,13]. Conversely, barrier compromise

and translocation of bacterial products such as lipopolysaccharide can trigger cytokine-mediated HPA activation [14,15]. Field-applicable indices of stress include plasma or fecal corticosterone, feather glucocorticoid deposition, and the heterophil–lymphocyte (H/L) ratio, each linked to fitness-relevant outcomes [16,17,18]. However, systematic microbiome data for the crested ibis are scarce, and transcriptionally informed functional profiles are particularly limited, constraining evidence-based health management.

Mechanistically, the avian gut microbiome supports host physiology by fermenting dietary carbohydrates to short-chain fatty acids (SCFAs), deconjugating and biotransforming bile acids, synthesizing amino acids and vitamins, and maintaining mucus and epithelial barriers [19,20]. Microbial metabolites, such as butyrate, propionate, indole derivatives, kynurenine-pathway products, signal through immune and neuroendocrine routes to shape innate and adaptive responses, stress recovery, energy allocation, and behavioral phenotypes [5,21,22]. Beyond the intestine, an intestine–liver–spleen–lung axis integrates mucosal and immunometabolic states: portal delivery of microbially derived molecules to the liver enables clearance and transformation. The spleen provides blood-borne immune surveillance, and the avian lung–air-sac system, continually exposed to bioaerosols, contributes to respiratory mucosal conditioning [23]. Accordingly, a multi-organ view anchored in the small intestine and extending to liver, spleen, and lung is well suited to establish a functional baseline for healthy ibises.

Captive environments can systematically reshape host–microbiome systems [24,25,26,27,28]. Diet homogenization and reduced foraging diversity are associated with lower α-diversity, community convergence, and depletion of fiber-fermenting symbionts [24,27]. These shifts can down-tune SCFA production and microbial bile-acid transformations, with consequences for mucosal nutrition and barrier tone [29,30]. Husbandry hygiene, disinfection, and water treatment alter exposure and colonization opportunities [31]. Prophylactic/therapeutic medications and feed additives impose direct selection and co-selection on the antibiotic-resistance gene (ARG) repertoire [32,33]. Biofilms in plumbing and drinking-water systems, together with mobile genetic elements (MGEs; integrases, transposases, conjugation/relaxase systems, plasmid replication/maintenance genes, and phage modules), facilitate horizontal gene transfer [31,34], contributing to distinctive resistome/mobilome profiles in captivity [32]. Overall, captivity tends to reduce diversity, shift key metabolic functions, and remodel resistance-related expression profiles.

Metatranscriptomics provides an RNA-centered view of function. By sequencing rRNA-depleted total RNA, it captures actively expressed microbial and viral transcripts and, in tissue-based sampling, can simultaneously profile host gene expression in the same libraries, enabling matched measurements of community composition, functional activity, and host response [23,35]. Compared with 16S rRNA amplicons or DNA-based metagenomics, metatranscriptomics more directly reflects real-time pathway activity and resolves expression of virulence and antimicrobial-resistance determinants. When paired with host profiling (dual RNA-seq), these signals can be mapped onto immune/inflammatory pathways in parallel [36,37]. For the crested ibis, multi-organ metatranscriptomics data from captive individuals can delineate a small-intestine–centered functional atlas and provide a practical framework for pathogen and resistance surveillance under husbandry conditions.

Against this background, we analyzed metatranscriptomes from the small intestine, liver, spleen, and lung from crested ibis specimens collected following acute stress–induced death to (i) define the transcriptionally active microbiome and core functional programs of the intestine; (ii) derive reference transcriptional footprints for detectable microbes and viruses in non-intestinal organs; and (iii) summarize pathogen-related markers and ARG/MGE expression to outline resistome features and detectability. Based on captivity effects reported in wildlife, we hypothesized lower expressed α-diversity and community convergence, with relative shifts in SCFA, bile-acid, tryptophan, and mucosa-associated pathways in the intestine, and low overall microbial expression in non-intestinal organs with occasional, reproducible low-level signals. These data are intended to inform health assessment, pathogen/resistance risk monitoring, and management interventions (diet optimization, water/enclosure hygiene, antimicrobial stewardship) in captive crested ibis.

2. Materials and Methods

2.1 Materials: Acquisition and Processing

Two captive female crested ibises (*N. nippon*) that died of stress-induced sudden death were sampled at necropsy under aseptic conditions. The small intestine was gently rinsed with RNase-free PBS to remove luminal contents; liver, spleen, and lung were blotted to remove surface blood. Tissues were placed in RNAlater or snap-frozen in liquid nitrogen and stored at −80 °C. Approximately 30–80 mg of each tissue was mechanically homogenized. Total RNA extraction, RNase-free DNase I treatment, RNA quality assessment, library preparation, and sequencing were performed by Nanchang Danong Biotechnology Co., Ltd. (Nanchang, Jiangxi, China) according to their standardized protocols. RNA integrity (RIN) and fragment profiles were assessed by the service provider as part of their standardized quality-control procedures. Libraries were prepared when RIN ≥6.0 and input RNA ≥500 ng. For Individual A, the four organs were processed and sequenced as separate libraries. For Individual B, equimass total RNA from the four organs was combined after DNase and QC to generate one pooled metatranscriptome library, which served as

a supplementary process-control sample for pipeline concordance rather than for organ-to-organ contrasts.

2.2 Meta-Transcriptomic Sequencing and Processing

To capture both host and microbial transcripts, rRNA depletion targeted eukaryotic (28S/18S) and prokaryotic (23S/16S/5S) rRNAs. Strand-specific (dUTP) paired-end libraries with unique dual indexes were prepared and sequenced on an Illumina platform (2×150 bp). Library preparation, sequencing, and initial bioinformatic processing were performed by Nanchang Danong Biotechnology Co., Ltd. (Nanchang, Jiangxi, China). For the four organ libraries shown in **Supplementary Fig. 1**, raw sequencing yields were approximately 14.7–28.0 million read pairs per library. FASTQ files were processed with fastp (OpenGene/HaploX Biotechnology, Shenzhen, Guangdong, China) for adapter removal, quality trimming (Q20 sliding window), poly-G/A trimming, and a minimum read length of 50 bp, while preserving read pairing.

For the microbial/viral analysis track, reads were mapped to the crested ibis reference genome/transcriptome (assembly/accession provided in **Supplementary Material**) using Bowtie2 (--very-sensitive-local). Read pairs with either mate aligning to host were discarded; unaligned pairs were retained as "non-host" reads. (When host expression summaries were required, the pre–de-host read set was quantified with Salmon using selective alignment and GC-bias correction.) Residual rRNA within the non-host set was removed with SortMeRNA (SILVA/RefSeq indices), yielding the working set for microbial taxonomic and functional profiling.

Taxonomic profiles were obtained with complementary methods: Kraken2 + Bracken (RefSeq, date-stamped) for species/strain-level assignments, and MetaPhlAn 4 for marker-based lineage profiling. To limit low-count noise, taxa meeting the tool-specific confidence criteria and supported by ≥10 assigned reads were summarized in the main results; sub-threshold signals are reported as exploratory "trace" calls in the Supplement. Microbial functional activity was profiled with HMP Unified Metabolic Analysis Network (HUMAnN) (bioBakery), mapping reads to UniRef protein families and regrouping to Kyoto Encyclopedia of Genes and Genomes (KEGG) and Metabolic Pathway Database (BioCyc) (MetaCyc) pathways; outputs include gene-family CPM/RPK and pathway relative abundance, optionally stratified by contributing taxa. For Gene Ontology (GO) annotation, HUMAnN-derived UniRef gene families were mapped to GO terms using the corresponding UniProt/GO annotations. Gene-family CPM values were aggregated by GO term and summarized separately for biological process (BP), molecular function (MF), and cellular component (CC). Both unstratified and taxon-stratified HUMAnN outputs were used for downstream descriptive summaries. Unstratified outputs supported KEGG/MetaCyc ranking and category-level overviews, whereas classified stratified outputs were used to summarize representative pathways, grouped functional axes, and taxon-level pathway/gene-family summaries. Viral signals were screened with Kraken2-viral and VirSorter2; candidates were considered "detected" only when supported by ≥10 reads and by at least one hallmark viral gene (e.g., capsid, polymerase, integrase); otherwise, they are presented as trace findings. Antimicrobial resistance (AMR) and mobilome profiling. ARGs were annotated with Resistance Gene Identifier (RGI) against the Comprehensive Antibiotic Resistance Database (CARD) and mobilome features were screened by hidden Markov model (HMM)/BLAST against curated marker sets (integrases, transposases, conjugation systems, plasmid markers, phage modules). Results are presented descriptively (presence/absence and normalized expression) without phenotypic risk inference. To increase robustness in low-abundance contexts, candidates (pathogens, viruses, ARGs) were retained only after coverage verification against references (≥10 non-redundant reads and ≥10% breadth, or ≥3 dispersed genes within the same genome/module) and cross-method concordance. Common low-biomass background taxa were reported as trace unless these criteria were met.

2.3 Statistical Analysis

Taxonomic abundances were normalized as RPM relative to the non-host, non-rRNA read denominator. Functional results are reported as gene-family CPM/RPK and pathway relative abundance. Diversity metrics (Shannon index, observed features) were computed from filtered tables. Community and pathway overviews were visualized with ordinations (e.g., PCoA on Aitchison or Bray–Curtis distances) for descriptive display. Given the design (four organ-specific libraries from Individual A plus one pooled library from Individual B), no hypothesis testing or effect-size estimation was performed; resistance and mobilome summaries are descriptive baselines. Raw FASTQ files, QC reports, and processed count tables will be deposited in a public repository (Genome Sequence Archive (GSA), PRJCA047134) together with metadata (individual ID, organ, sampling details, RNA QC, library/sequencing metrics, and database versions). Because organ-resolved libraries were available for only one individual, all functional visualizations and taxon-stratified summaries were treated as descriptive rankings and compositional summaries, without formal enrichment testing or inferential statistics.

3. Results

3.1 Dataset and Analytical Workflow

We generated a multi-organ metatranscriptomic dataset from two captive female crested ibises that experienced stress-induced sudden death. Individual A yielded organ-resolved libraries for the small intestine, liver, spleen, and lung. Individual B contributed an equal-mass RNA pool from the same four organs as a single supple-

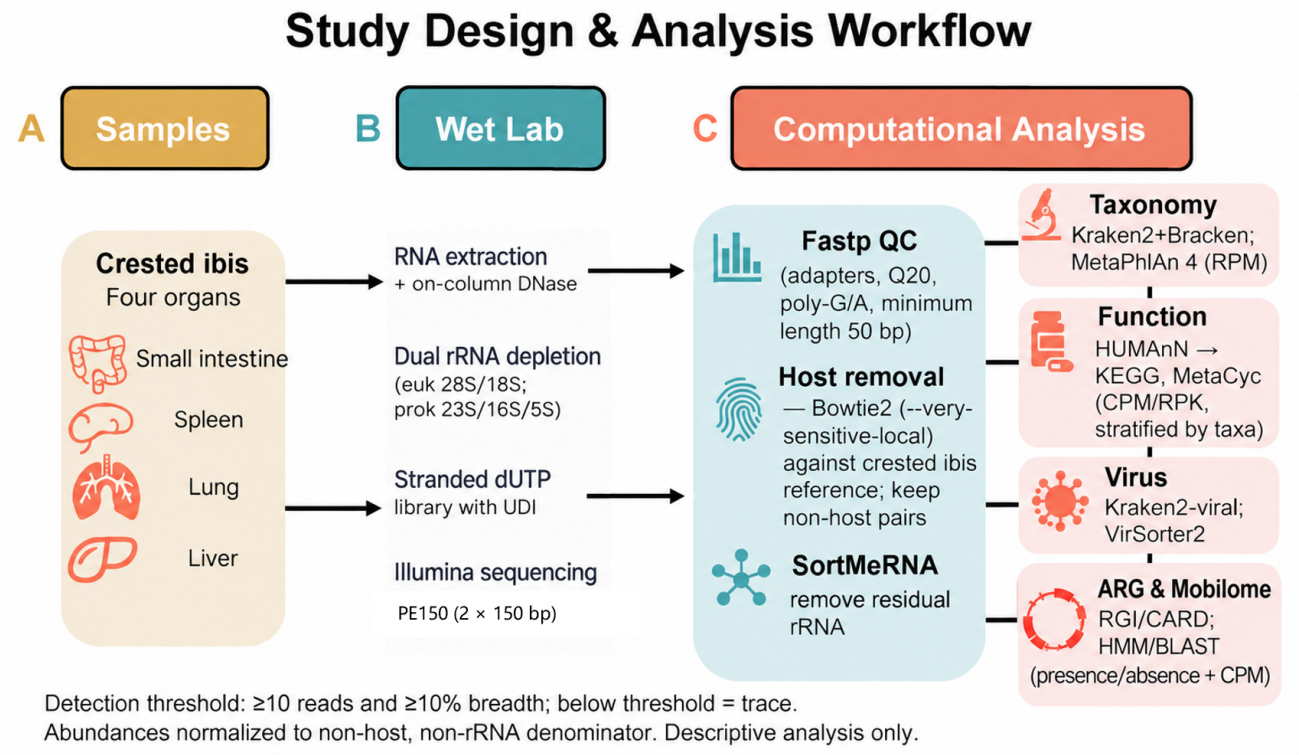

Fig. 1. Study design and analysis workflow. (A) Sampling scheme. Two captive female crested ibis (*Nipponia nippon*). Individual A: organ-specific libraries from small intestine, liver, spleen, and lung. Individual B: the four organs pooled in equal mass as a process control (used for pipeline comparison, not for organ-to-organ contrasts). (B) Wet-lab overview. Total RNA extraction with on-column DNase → dual rRNA depletion (prokaryotic + eukaryotic) → strand-specific library construction → Illumina paired-end sequencing. (C) Computational workflow. Read QC (fastp) → host subtraction against the N. nippon genome (Bowtie2) → residual rRNA removal (SortMeRNA) → parallel analyses: taxonomic profiling (Kraken2/Bracken; MetaPhlAn 4), functional profiling (HUMAnN to KEGG and MetaCyc; GO mapping), viral screening (Kraken2-viral; VirSorter2), and resistome/mobilome screening (RGI/CARD). Abundances are normalized to the non-host, non-rRNA read denominator. For low-biomass viscera (liver/spleen/lung), common background taxa were conservatively masked; only features passing coverage checks and showing cross-method concordance are retained. Detection threshold used throughout the manuscript: ≥10 supporting reads and ≥10% reference breadth (as applicable). All downstream results are descriptive (per-organ n = 1). HUMAnN, HMP Unified Metabolic Analysis Network; KEGG, Kyoto Encyclopedia of Genes and Genomes; MetaCyc, Metabolic Pathway Database (BioCyc); GO, Gene Ontology; RGI, Resistance Gene Identifier; CARD, Comprehensive Antibiotic Resistance Database.

mentary library used to check pipeline concordance, not for organ-to-organ contrasts (Fig. 1). After standard library preparation and Illumina paired-end 150 bp (PE150) sequencing (Methods), reads were processed with a unified pipeline: fastp for quality control and adaptor trimming, Bowtie2 to remove host-mapped reads against the crested ibis reference, and SortMeRNA to filter residual rRNA. Downstream analyses proceeded along four branches (Fig. 1), including (1) Taxonomy: Kraken2 + Bracken and MetaPhlAn 4. (2) Function: HUMAnN with regrouping to KEGG/MetaCyc pathways. (3) Virus: Kraken2-viral and VirSorter2. (4) Antibiotic resistance/mobilome: RGI/CARD complemented by curated HMM/BLAST marker sets (integrases, transposases, conjugation/relaxase systems, plasmid replication/maintenance genes, and phage modules).

Relative abundances were normalized to the non-host, non-rRNA read total. To limit false positives in low-biomass tissues, a feature was called detected only if supported by ≥10 reads and ≥10% reference breadth (or, for multi-gene modules, ≥3 dispersed genes); sub-threshold signals were flagged as trace. Analyses are descriptive given the organ design (n = 1 per organ for Individual A) and the conservative reporting criteria. All libraries passed basic QC: high per-base Phred scores across cycles, negligible adapter signal, expected GC ranges (≈45–53%), and uniform 150-bp read length (**Supplementary Fig. 1A–E**).

3.2 Microbial Composition and Diversity Across Organs

Following the unified reporting scheme (normalization to the non-host, non-rRNA denominator; Detected = ≥10 supporting reads and ≥10% genomic breadth), genus-

and family-level compositions showed strong organ specificity: the small intestine was dominated by a few gut-typical taxa, whereas liver, spleen, and lung exhibited low overall abundance and sparse communities (Fig. 2A,B). A genus-level measure of relative microbial transcriptional signal (the sum of microbe-assigned reads per million (RPM), plotted as $\log_2$) showed that microbial activity was concentrated in the intestine (small intestine = 480,502 RPM; liver = 124; spleen = 543; lung = 739; Fig. 2C). Pairwise β-diversity distances varied markedly among organs (Aitchison and Bray–Curtis; Fig. 2D,E). The liver was consistently among the most compositionally divergent samples, whereas the spleen and lung were relatively closer; notably, the small intestine was highly dissimilar to the liver but much closer to the lung.

For cross-organ occupancy, using a lenient presence cutoff of RPM ≥5, we observed 18 genera in total. Only four non-zero intersection classes were detected: small intestine-specific genera were most numerous (n = 8), followed by the small intestine + lung intersection (n = 5), liver-specific genera (n = 3), and the small intestine + spleen + lung intersection (n = 2) (Fig. 2F). Thus, genera shared by three organs accounted for 2/18 (11%), whereas no genus was shared across all four organs. An occupancy-ordered presence/absence heatmap corroborated this pattern: most genera were confined to—or dominated by—the intestine, with few reproducibly detected across liver, spleen, and lung (Fig. 2G).

Within the small intestine, the leading detected taxon was *Cetobacterium somerae* (54.83%). This freshwater-associated commensal is known for vitamin B_{12} and acetate production and for links to host carbohydrate metabolism. Its dominance aligns with captive fish-based feeding records (e.g., loaches), indicating a stable aquatic input [38,39]. Several clostridial-related taxa occurred at lower relative abundance, including *Paraclostridium sordellii* (3.10%), *P. bifermentans* (1.27%), *P. ghonii* (0.44%), and *Clostridium perfringens* (1.10%).

These groups carry toxin potential and are typically opportunistic/conditionally pathogenic. Notably, *C. perfringens* can cause necrotic enteritis in birds, representing a background risk signal here [40]. Additional opportunists included *Fusobacterium nucleatum* (1.11%), *Clostridioides difficile* (0.64%), and *Plesiomonas shigelloides* (0.41%), the latter often linked to water hygiene, consistent with the aquatic signal. Conversely, butyrate-associated taxa such as *Romboutsia spp*. were low (0.27%), suggesting limited butyrogenic potential and, by implication, a comparatively weaker anti-inflammatory/ barrier-supporting capacity at baseline.

Across liver/spleen/lung, reproducibly detected taxa were few and discrete. Dominant signals were carried by a small number of genera and were concordant across classifiers, whereas many low-count entries were treated as trace or grouped into Others (Fig. 2A,B). These patterns mirror the β-diversity results (Fig. 2D,E) and support low-load, low-sharing active microbiomes in viscera. All findings are descriptive. For low-biomass tissues, only coverage-verified and cross-method-concordant taxa are emphasized in the main text. Ecological and functional implications are pursued in the pathway-level analyses.

3.3 Functional Profiles of the Small Intestine

Consistent with the intestine-centered microbial activity observed in Fig. 2, the small-intestine metatranscriptome showed a broadly metabolism-oriented functional profile. In the KEGG summaries (Fig. 3A,B), the highest-ranked signals were distributed across amino-acid turnover, nucleotide-related reactions, redox-associated enzymes, and central carbon processing, rather than being concentrated in a single dominant pathway class. Representative high-ranking entries included glycine reductase components, methylaspartate mutase, adenylate kinase, ornithine carbamoyltransferase, arginine deiminase, glyceraldehyde-3-phosphate dehydrogenase, and ferredoxin/flavodoxin–$NADP^+$ reductase, together indicating active substrate conversion, energy-linked redox handling, and precursor turnover in the small intestine.

From the MetaCyc perspective, the same overall structure was retained. At the category level (Fig. 3C), pathways grouped as "Other" constituted the largest fraction (41.7%) of total pathway abundance. Among the explicitly defined major metabolic categories, nucleotide/cofactor/vitamin metabolism accounted for the largest share of annotated pathway abundance, followed by amino-acid and carbohydrate metabolism, whereas lipid/fatty-acid and cell wall/envelope pathways formed smaller but still visible components. At the pathway level (Fig. 3D), the most prominent signals clustered into several recurring themes, including nucleotide salvage and turnover, central carbon conversion, cofactor supply, and envelope-associated precursor synthesis. These results together outline a functional baseline centered on substrate use, precursor regeneration, and maintenance of cell-surface structures.

Taken together, the unstratified KEGG and MetaCyc results support a small-intestine program organized around three broad functional tendencies: ongoing small-molecule metabolism, active cofactor and nucleotide turnover, and sustained investment in membrane/envelope-associated precursor pathways. This organization is consistent with a lumen-exposed microbial community engaged in nutrient processing while maintaining its cellular interface. High-level GO summaries (**Supplementary Fig. 2A–C**) remained concordant with this framework, with metabolism-, redox-, transport-, and membrane-associated terms occupying the dominant positions across ontology categories. The unstratified category-to-pathway allocation (**Supplementary Fig. 3**) likewise supported the same broad architecture from a higher-level summary view. All statements are descriptive and confined to the single small-

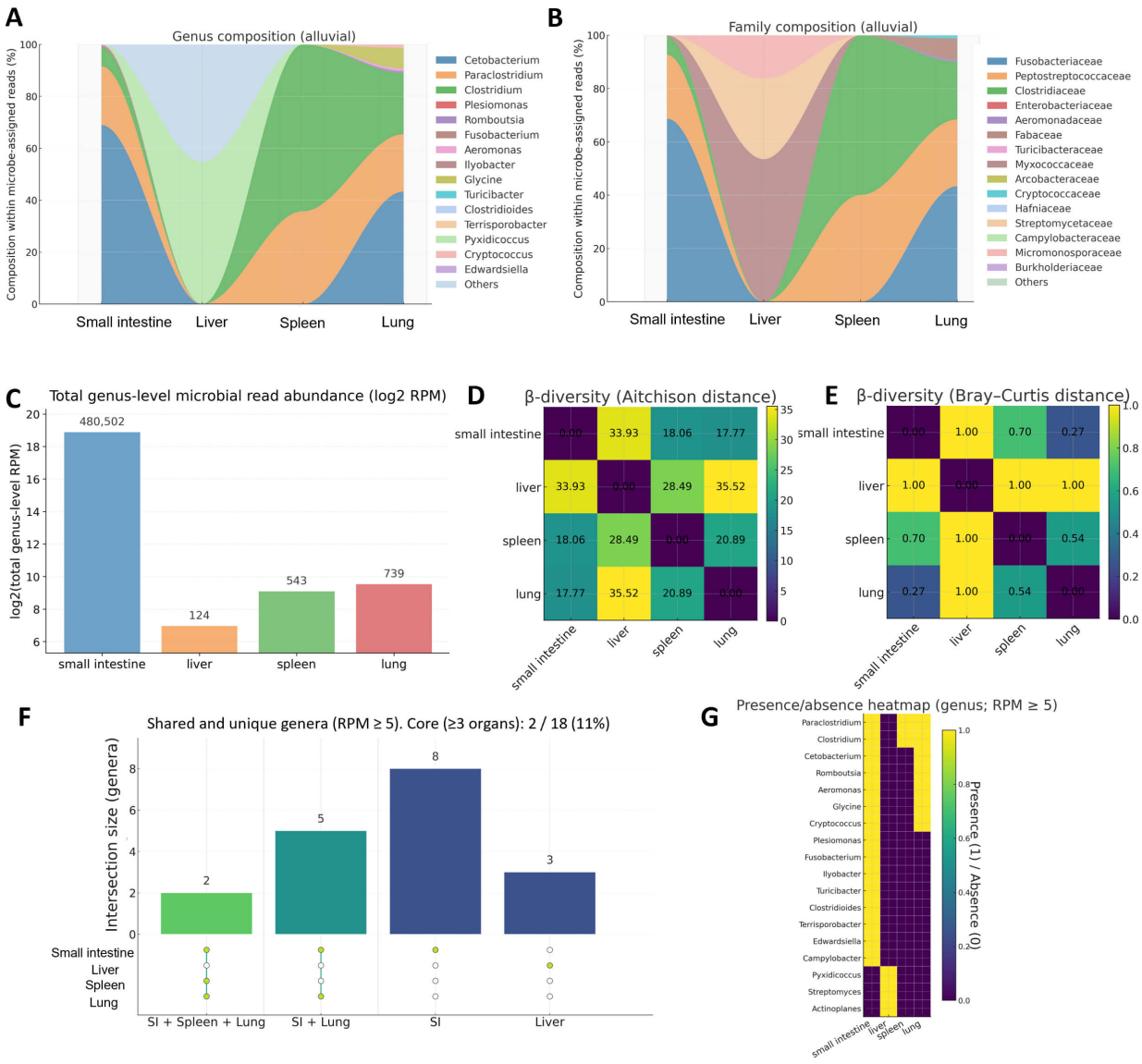

Fig. 2. Microbial composition across organs. (A) Genus composition (alluvial). Taxonomic profiling with Kraken2 (PlusPF) followed by Bracken re-estimation. Abundances were summed at the genus level, converted to relative abundance, and plotted as percentages within microbe-assigned reads (residual taxa collapsed as Others). (B) Family composition (alluvial). Same workflow as in (A), summarized at the family level. (C) Relative microbial transcriptional signal. Total genus-level RPM per sample is shown on a log2 scale; labels above bars indicate the corresponding untransformed RPM values. The small intestine shows the highest relative microbial transcriptional signal. (D) β-diversity (Aitchison distance). Genus-level abundance matrices were CLR-transformed and Euclidean distances computed; values are shown as a heatmap. (E) β-diversity (Bray–Curtis distance). Bray–Curtis distances were calculated from genus-level relative abundances and displayed as a heatmap. (F) Shared and unique genera (UpSet-style bars). "Presence" was defined as RPM ≥5. Bar heights indicate set sizes across organs; the caption reports the size of the core set (detected in ≥3 organs). (G) Presence/absence heatmap (genus; threshold RPM ≥5). Binary heatmap (1/0) illustrating organ-specific and shared genera. Notes: All samples underwent quality control, host and rRNA read removal, and exclusion of Homo/Nipponia-related hits prior to profiling. Percentages in (A,B) are computed relative to microbe-assigned reads only. RPM, reads per million (normalized to non-host, non-rRNA reads); CLR, centered log-ratio.

intestine library in Fig. 3. Abundances are normalized to the non-host, non-rRNA denominator, and features are reported under the manuscript-wide detection criteria (≥10 supporting reads and ≥10% genomic breadth; species stratification only where adequately supported). Cross-organ functional contrasts are not presented here given the low biomass in viscera. Unstratified abundance tables for KEGG KOs (CPM; housekeeping filtered), MetaCyc

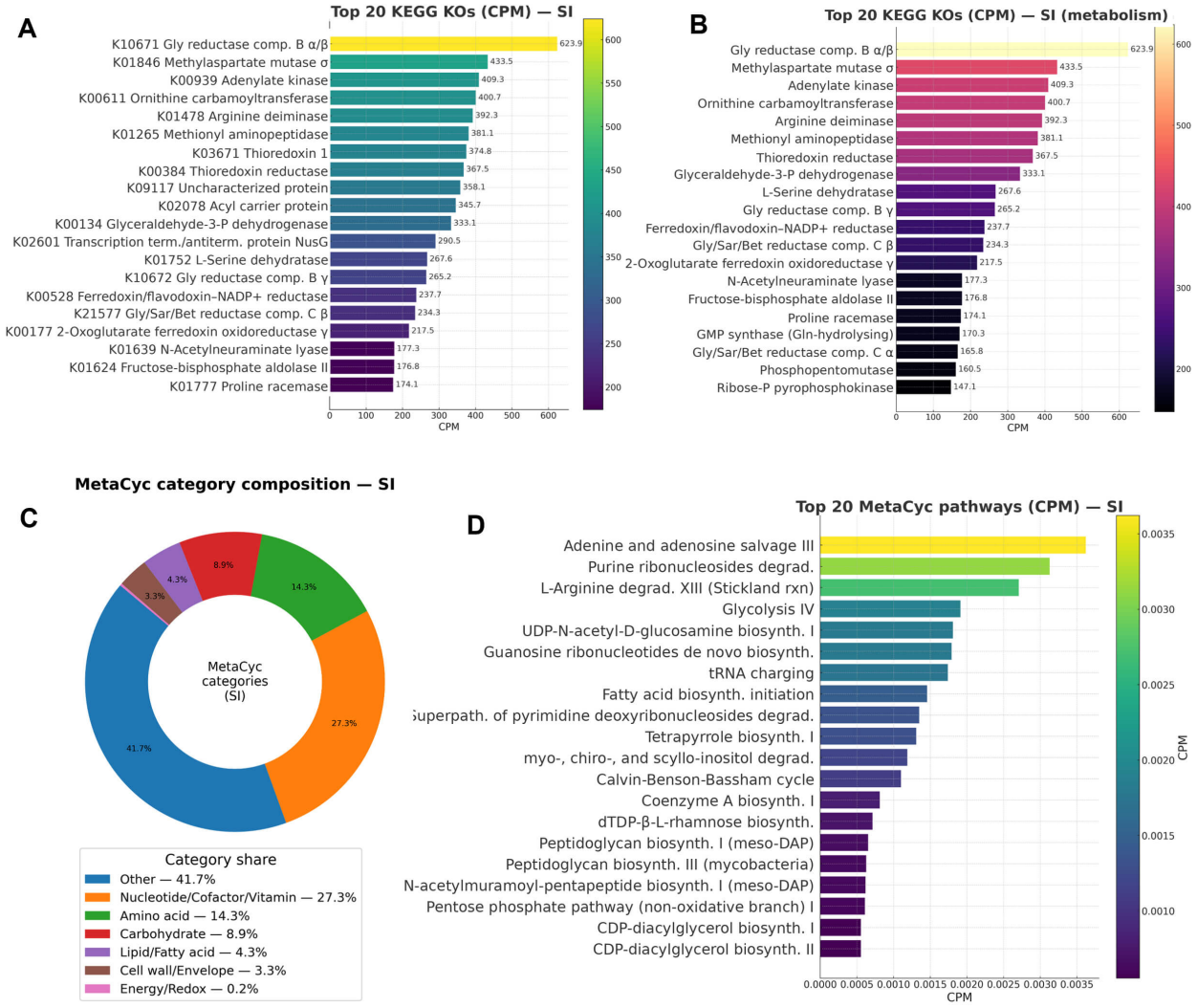

Fig. 3. Unstratified functional profile of the small-intestine metatranscriptome. (A) Top 20 KEGG orthologs (KOs) ranked by abundance in the small-intestine metatranscriptome. (B) Top 20 metabolism-related KEGG orthologs after restricting the analysis to metabolic functions. (C) Relative contribution of major MetaCyc pathway categories in the small intestine, showing the overall functional allocation among nucleotide/cofactor/vitamin, amino-acid, carbohydrate, lipid/fatty-acid, and cell wall/envelope-associated pathways. (D) Top 20 MetaCyc pathways ranked by abundance in the small-intestine metatranscriptome. Notes (all panels). Derived from HUMAnN unstratified output for the SI sample; Y-axis labels are abbreviated for readability; full pathway names are provided in **Supplementary Table 1**.

pathways (CPM with category assignment), and GO terms (BP/MF/CC; CPM and percent contribution) are available as **Supplementary Tables 2–4**.

3.4 Taxon-Stratified Functional Architecture of the Small Intestine

To further resolve how the small-intestine functional baseline was distributed across classified contributors, we summarized the stratified HUMAnN results for the major taxa that were reproducibly resolved in this library, namely *Cetobacterium somerae*, *Paraclostridium bifermentans*, and *Clostridium perfringens* (Fig. 4A–C). Rather than assigning the pathway signal to a single dominant taxon, the classified fraction revealed a partitioned metabolic program in which multiple contributors supported the same overall organization observed at the community level.

At the representative-pathway level (Fig. 4A), *Paraclostridium bifermentans* represented the broadest classified contributor. Its signal extended across the main functional axes already highlighted in the unstratified small-intestine profile, including nucleotide turnover, central carbon conversion, cofactor supply, and envelope-associated precursor synthesis. This broad distribution indicates that part of the small-intestine metabolic background was carried by a taxon with wide pathway coverage rather than by a narrowly specialized contributor.

By contrast, *Cetobacterium somerae* contributed more prominently to the nucleotide-linked portion of the clas-

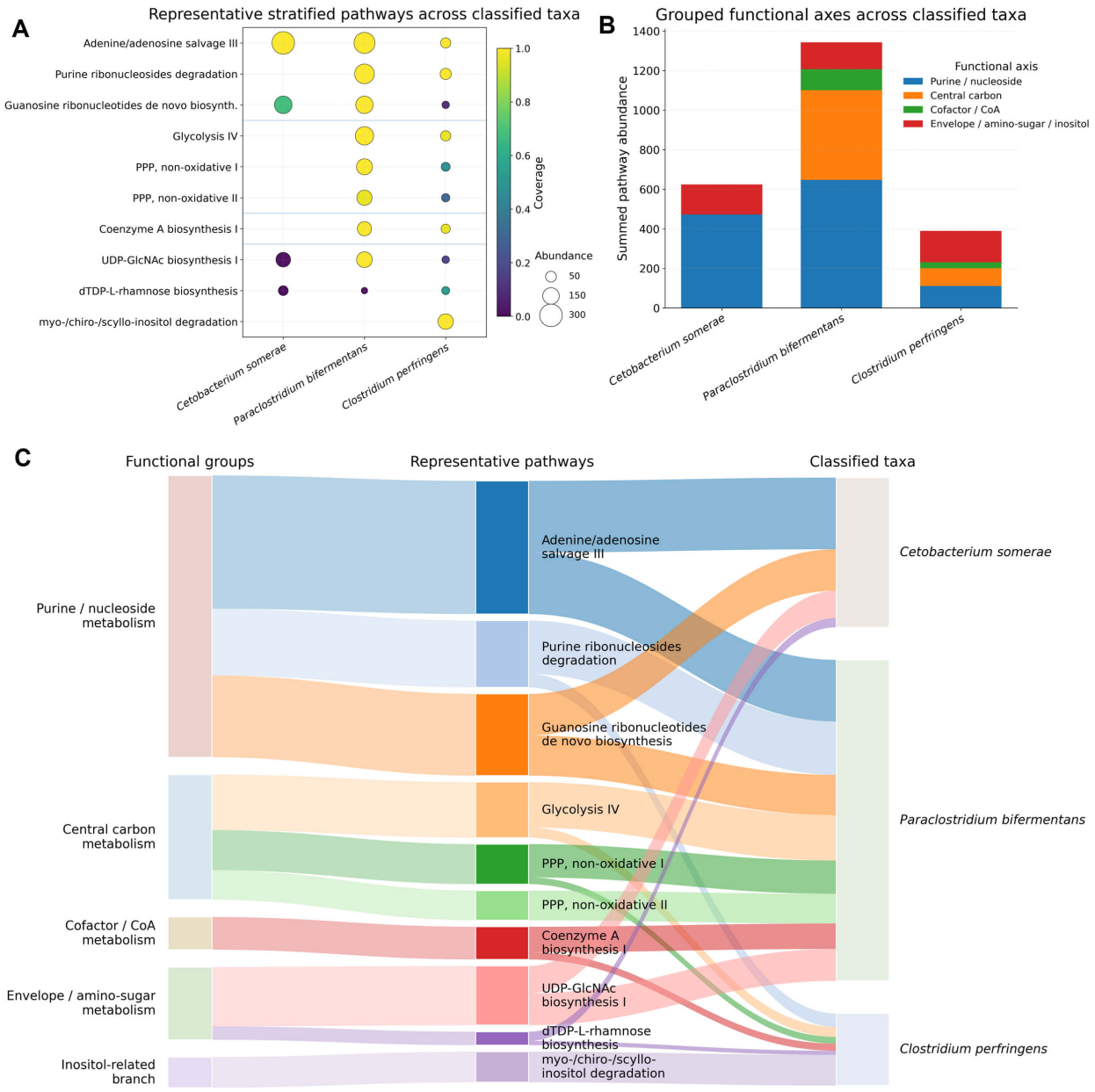

Fig. 4. Taxon-stratified functional architecture of the small-intestine metatranscriptome. (A) Representative stratified pathways across classified taxa. Bubble plot summarizing 10 representative MetaCyc pathways assigned to the three reproducibly classified contributors in the small-intestine library: *Cetobacterium somerae*, *Paraclostridium bifermentans*, and *Clostridium perfringens*. Horizontal separators group pathways into major functional themes, including purine/nucleoside metabolism, central carbon metabolism, cofactor/CoA metabolism, envelope/amino-sugar metabolism, and the inositol-related branch. (B) Grouped functional axes across classified taxa. Stacked bar plot showing summed pathway abundance after grouping the representative pathways into four higher-level axes: purine/nucleoside, central carbon, cofactor/CoA, and envelope/amino-sugar/inositol. This panel summarizes the relative contribution of each classified taxon to the major functional structure recovered in the stratified output. (C) Functional allocation across classified taxa. Integrated flow diagram linking broad functional groups to representative pathways and then to classified taxa. Only the major classified links were retained to emphasize preferential pathway weighting across taxa rather than exhaustive pathway assignment. Together, the three panels show that the classified fraction of the small-intestine functional profile is organized as a shared metabolic framework with uneven contributions from different taxa.

sified profile, especially in salvage- and ribonucleotide biosynthesis-related routes, while remaining less broadly distributed across the other functional branches (Fig. 4A). *Clostridium perfringens* showed a more localized pattern, with its clearest contribution mapping to the inositol-related branch, although it also overlapped with several shared

purine- and carbon-associated pathways (Fig. 4A,C). When the same pathways were grouped into broader functional categories, purine/nucleoside metabolism remained the largest classified component across taxa, and Paraclostridium bifermentans remained the dominant classified contributor overall (Fig. 4B). Taken together, these results indicate that the classified component of the small-intestine metatranscriptome was organized as a shared core metabolic framework with uneven pathway weighting across taxa, rather than as a uniform or taxon-exclusive system.

This interpretation was further supported by the taxon-level summaries (**Supplementary Fig. 4A,B**). *Cetobacterium somerae* contributed the highest overall stratified gene-family abundance, whereas *Paraclostridium bifermentans* and *Clostridium perfringens* spanned broader pathway repertoires. Thus, overall transcript-weighted dominance and pathway-repertoire breadth did not fully coincide in the small intestine. At the same time, the unclassified fraction remained substantial, indicating that the resolved classified architecture captured an important but still incomplete subset of the small-intestine functional landscape.

3.5 Antimicrobial Resistance–Associated Transcripts

In the small-intestine library, the distribution of AMR-associated gene–drug-class assignments displayed a "single-peak + long-tail" profile at the drug-class level, with elfamycin dominating (~77%) and glycopeptide secondary (~14%), while fluoroquinolone, nybomycin-like, and MLS-related classes each contributed small, dispersed fractions (typically 1–3%; Fig. 5A). At the gene level (Fig. 5B), read contributions were concentrated in a few targets: EF-Tu variants paired with elfamycin formed the global maximum; *rpoC* (RNA polymerase β′) mapped to glycopeptide as a second tier; *gyrA* (fluoroquinolone target) was consistently present but modest; and ErmQ (23S rRNA methyltransferase) appeared at low abundance across MLS branches. The hierarchical mapping (Fig. 5C) separates target-site modification (single-class links for EF-Tu with elfamycin and rpoC with glycopeptide, with gyrA linked to both fluoroquinolone and nybomycin-like antibiotics) from ribosomal methylation (ErmQ to MLS, one-to-many via the 23S methylation family). Evidence metrics (reads, coverage, model support) converged on the ranking EF-Tu ≫ *rpoC* > ErmQ > *gyrA* (Fig. 5D).

Functionally, this pattern is most consistent with allelic variation and background expression of core targets (translation elongation factor, RNA polymerase, DNA gyrase) rather than dominance of acquired enzymatic inactivation. That emphasis aligns with the intestinal functional landscape described earlier and high investment in translation/central metabolism, nucleotide turnover, and envelope renewal/transport, in which elevated demand on core information-processing and cell-surface maintenance would proportionally weight transcripts from EF-Tu, *rpoC*, and *gyrA*. By contrast, ErmQ shows the expected low-level, broad coverage typical of widely distributed MLS methyltransferases. The full per-gene AMR evidence (**Supplementary Table 5**) and a threshold sensitivity check confirming pattern robustness (**Supplementary Fig. 5**) are provided.

4. Discussion

The main contribution of this study is the establishment of an organ-resolved metatranscriptomic reference for the crested ibis under conditions in which systematic sampling is intrinsically limited. The individuals analyzed here were derived from cases consistent with previously characterized stress-associated sudden death in this species, as supported by prior behavioral, pathological, and endocrine evidence, including abnormal corticosterone baseline profiles [41]. The dataset is therefore best interpreted as a descriptive, hypothesis-generating baseline rather than a population-level account of the species microbiome. Even within that scope, however, the data define a clear internal structure: microbial transcription was concentrated in the small intestine, whereas liver, spleen, and lung showed uniformly low-load and weakly shared signals. This spatial contrast indicates that active microbial expression in the present material was primarily an intestinal phenomenon, while the extra-intestinal organs were characterized by a low-background state that can serve as an internal reference for interpreting future microbial shifts outside the gut. Within this gut-centered structure, the intestinal profile is compatible with an ecological setting shaped by fish-based feeding, repeated water exposure, and relatively stable husbandry conditions. The predominance of *Cetobacterium somerae* is consistent with such a context, although the absence of matched controls does not allow this pattern to be assigned specifically to captivity. In this setting, *C. somerae* is informative not only because of its abundance, but also because it links the intestinal microbiome to a recognizable aquatic and dietary background. Its reported associations with aquatic vertebrates, cobalamin production, and acetate-linked metabolism suggest that recurrent environmental and dietary inputs are likely to contribute to the organization of the small-intestine community [38,39]. Thus, the gut signal can be read as an ecologically interpretable microbial profile, while the extent to which it reflects captivity-specific filtering remains to be tested in future comparative sampling.

The functional architecture of the small intestine extends this ecological reading. The dominant KEGG and MetaCyc signals converge on small-molecule metabolism, nucleotide/cofactor turnover, central carbon conversion, and membrane/envelope-associated precursor pathways. Together, these categories define a mucosal metabolic program rather than a narrow single-pathway specialty. Such a program is biologically coherent for an intestinal habitat, where microorganisms must continuously transform in-

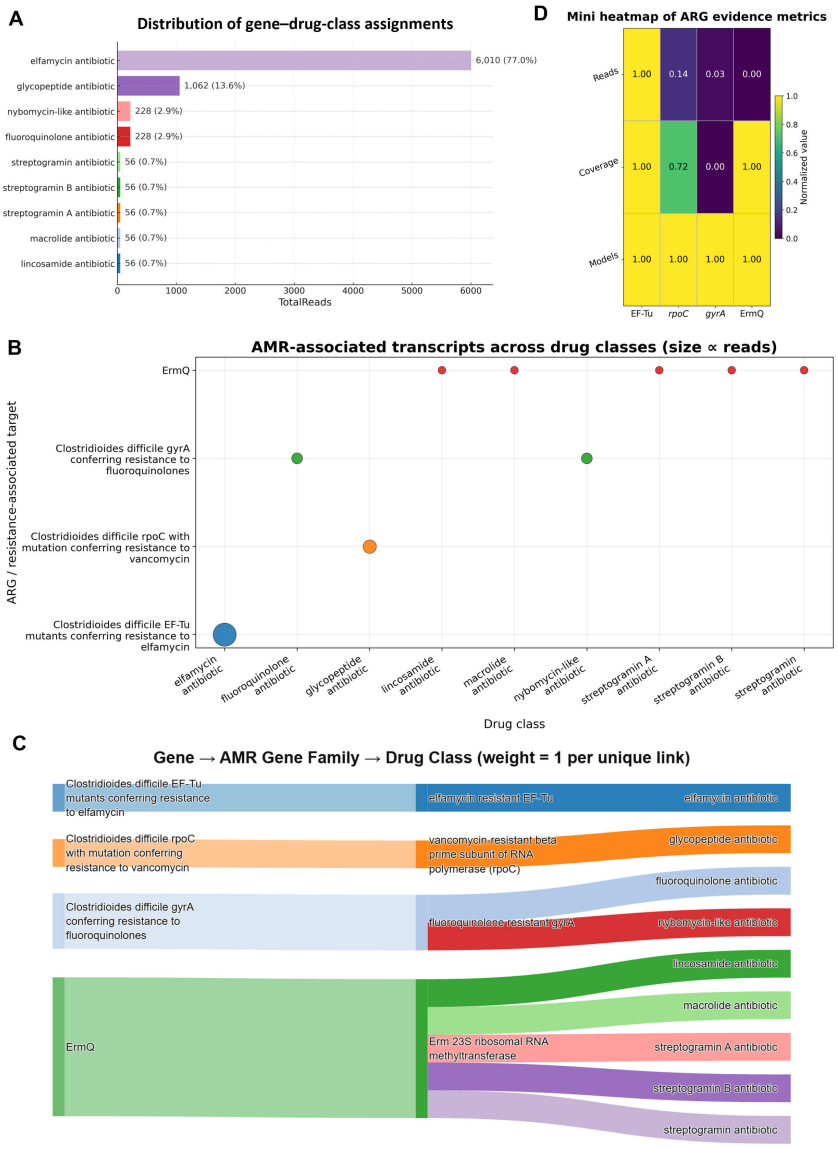

Fig. 5. AMR-associated transcription in the small-intestine metatranscriptome. Analysis is limited to the small-intestine library. Abundances are normalized to non-host, non-rRNA reads. Only features meeting the detection threshold (≥10 supporting reads and ≥10% breadth) and cross-method concordance are shown. MLS denotes macrolide–lincosamide–streptogramin. (A) Distribution of gene–drug-class assignments. Read counts associated with each resistance-related gene were assigned to all corresponding drug classes; therefore, genes linked to multiple drug classes contribute to more than one category. Percentages were calculated relative to the summed gene–drug-class assignment count (n = 7808), rather than the 7356 unique gene-associated reads. The profile was dominated by elfamycin-associated assignments (77.0%), followed by glycopeptide-associated assignments (13.6%), with smaller contributions from fluoroquinolone and nybomycin-like antibiotics (2.9% each) and MLS-related classes (0.7% each). (B) AMR-associated genes across drug classes. Bubble size reflects gene-level reads within the corresponding class. Four entries account for most signal: EF-Tu variants → elfamycin (global maximum); *rpoC* (RNA polymerase β′) → glycopeptide (second tier); *gyrA* → fluoroquinolone (lower but consistent); ErmQ → MLS (cross-branch, low per-class reads). Overall pattern: one strong (EF-Tu/elfamycin) + two moderate (*rpoC*, *gyrA*) + one broad (ErmQ/MLS). (C) Gene → AMR gene family → Drug class (Sankey). Hierarchical mapping with unit link weight (=1). Most pairs are one-to-one (EF-Tu↔elfamycin; *rpoC*↔glycopeptide); ErmQ connects one-to-many to MLS via the 23S rRNA methylation family; *gyrA* maps to both fluoroquinolone and nybomycin-like antibiotic classes. This separates target-site modification (*gyrA*/*rpoC*/EF-Tu) from ribosomal methylation (ErmQ). (D) Mini heatmap of ARG evidence metrics. Three evidence dimensions (Reads, Coverage, Models) are 0–1 scaled, providing complementary support for the four gene-level signals. EF-Tu scores high on all metrics; *rpoC* shows good coverage/model support with moderate reads; ErmQ is low-abundance but well supported; *gyrA* is low reads/coverage yet above the detection threshold—corroborating panels (A–C).

coming substrates, maintain reducing equivalents and cofactor supply, and renew cell-surface structures under constant exposure to bile, host secretions, and other chemical pressures [29,30]. The repeated prominence of nucleotide and cofactor metabolism is particularly notable, because it indicates that intestinal activity is sustained not only by substrate flow itself, but also by continued investment in the biochemical infrastructure required to support that flow. In parallel, the strong representation of envelope-associated precursor pathways suggests that surface maintenance is integral to the intestinal state rather than secondary to it.

Viewed from the perspective of carbon handling, the intestinal configuration is also informative for how microbial metabolism may be balanced at the mucosal interface. The prominence of *Cetobacterium* together with strong central-carbon processing is consistent with a system in which rapid carbon throughput is a major feature. At the same time, the overall community structure does not resemble a strongly fiber-fermentative configuration dominated by classical butyrate-associated guilds. Instead, it is more compatible with an intestinal environment in which acetate-linked metabolism, cofactor-intensive processing, and membrane renewal are especially prominent, while butyrogenic buffering occupies a less dominant position. For a mucosal habitat, this balance is likely to matter because it ties together energy handling, barrier support, and the chemical tone of the gut environment [29,38].

The classified pathway structure further shows that this intestinal program is carried by a functionally layered community rather than by a single dominant lineage alone. *Paraclostridium bifermentans* spans the broadest classified pathway repertoire and extends across nucleotide turnover, central carbon metabolism, cofactor supply, and envelope-associated precursor synthesis, indicating that it contributes much of the breadth of the intestinal functional system. *Cetobacterium somerae* remains a major contributor, but its classified signal is weighted more strongly toward the nucleotide-linked sector, whereas *Clostridium perfringens* occupies a narrower position centered most clearly on the inositol-related branch. The supplementary taxon-level overview adds another dimension by showing that transcript-weighted abundance and pathway breadth do not fully coincide: *Cetobacterium* dominates total classified gene-family abundance, whereas *Paraclostridium* and *C. perfringens* cover broader classified repertoires, and an unclassified fraction remains substantial. The intestinal baseline is therefore best understood as a composite system in which dominant output, distributed functional breadth, and unresolved background coexist within the same community.

This layered organization also gives clearer meaning to the lower-abundance taxa. In the small intestine, taxa such as *Paraclostridium* spp. and *Clostridium perfringens* are better regarded as structured secondary contributors than as incidental background, because they expand the functional envelope of the community and help define its internal organization. At the same time, water-associated and opportunistic taxa such as *Plesiomonas shigelloides*, *Clostridioides difficile*, and *Fusobacterium nucleatum* may reflect environmental exposure, habitat filtering, and husbandry context rather than overt pathology [42]. Their value lies less in implying overt pathology than in recording the kinds of ecological inputs that move through the intestinal system under the present conditions. This supports an interpretation of the intestinal microbiome away from isolated taxa and toward a broader ecological assembly shaped by diet, water source, enclosure conditions, and microbial opportunity.

The low-load profile of liver, spleen, and lung extends the same logic to the rest of the body. These organs do not display a transcriptionally prominent microbial program comparable to that of the small intestine. Instead, they define a low-background state across the intestine–liver–spleen–lung axis. That background is useful precisely because it is quiet: in endangered species medicine, where repeated destructive sampling is rarely possible, a stable low-signal baseline can serve as an internal reference against which future deviations become interpretable. A reproducible microbial signal outside the gut may therefore be meaningful not because extra-intestinal colonization is expected as a default condition, but because it stands out against an otherwise low-transcription setting. In this sense, the visceral organs function less as co-equal microbial habitats and more as sensitive sentinel compartments within a gut-centered system.

The AMR-associated transcript profile fits naturally into this broader ecological and functional frame. The dominance of EF-Tu-, *rpoC*-, and *gyrA*-linked targets, together with a low-level ErmQ-associated MLS component, places the major detectable resistance-related transcription within the same intestinal compartment that also carries the strongest metabolic and structural activity. The resistome signal is therefore best read as part of the intestinal background shaped by exposure history and community state, rather than as an independent layer detached from the rest of the microbiome. For conservation monitoring, this is a useful arrangement: ARG expression can be tracked alongside taxonomy and pathway activity as part of a surveillance-oriented baseline, while isolate-based susceptibility testing remains necessary for evaluating phenotypic resistance in veterinary practice [31,32,33,34].

Taken together, these findings support a coherent view of the crested ibis microbiome under the present sampling conditions as an ecologically interpretable, intestine-centered, functionally stratified system. The small intestine emerges as the dominant active compartment, associated with identifiable dietary and aquatic inputs and organized around continuous metabolic processing, cofactor turnover, and interface maintenance. The visceral organs provide the complementary low-background frame of reference against

which future change may be judged. Within that architecture, the resistome appears as a contextual layer rather than a separate narrative. This integrated view is likely to be more informative for conservation physiology than any single taxonomic or pathway signal in isolation, because it offers a structured baseline against which captive–wild comparisons, longitudinal monitoring, and targeted physiological validation can be interpreted.

A natural next step is to test this architecture across biological and management gradients rather than treating it as a static endpoint. The most informative extension would be a comparative framework spanning captive, semi-wild, and wild birds, ideally combined with repeated non-lethal sampling and targeted measurements of metabolites, sentinel taxa, and ARGs. Such a design would allow the present structure to be evaluated for stability, plasticity, and management relevance across season, diet, reproductive stage, treatment history, and habitat regime. In that broader setting, the value of the present study is that it already provides a workable internal map of microbial activity and function in the crested ibis, one that can anchor future ecological, veterinary, and conservation-oriented investigations.

5. Limitations

Several considerations should be taken into account when interpreting these findings. Owing to the opportunistic nature of post-mortem sampling in this endangered species, the cohort was limited, and organ-resolved libraries were available from one individual, while the pooled library from the second individual served primarily as a process control. The observed patterns should therefore be regarded as an initial, context-specific reference rather than a population-level baseline. In addition, microbial signals in the liver, spleen, and lung were substantially lower than those in the intestine; despite conservative detection criteria, their biological significance will require confirmation using larger cohorts, appropriate technical controls, and absolute quantification. Finally, pathway and antimicrobial-resistance annotations were based on computational inference from metatranscriptomic data and were not validated by metabolomics, microbial culture, or susceptibility testing. Future studies integrating broader biological replication, matched ecological controls, and complementary multi-omic measurements will help determine the stability and physiological relevance of these observations.

6. Conclusions

This study establishes the first organ-resolved metatranscriptomic baseline for the crested ibis and identifies a clear intestine-centered organization of microbial activity across the sampled organs. The small intestine carried the dominant microbial transcriptional burden, whereas liver, spleen, and lung remained low-load and weakly shared, defining a contrasting extra-intestinal background. Within the intestine, the active microbiome was characterized by *Cetobacterium somerae* dominance together with a metabolism-centered functional profile enriched in small-molecule metabolism, nucleotide/cofactor turnover, central carbon conversion, and membrane/envelope-associated precursor pathways. Taxon-stratified analysis further showed that this intestinal functional baseline was not carried by a single lineage alone, but by a layered community in which *Paraclostridium bifermentans* contributed broad pathway coverage, *Cetobacterium somerae* was more strongly weighted toward nucleotide-linked functions, and *Clostridium perfringens* retained a more localized contribution. In parallel, AMR-associated transcripts in the intestine were dominated by target-linked signals such as EF-Tu, *rpoC*, and *gyrA*, with a low-level ErmQ-associated MLS component, supporting their interpretation as contextual markers of community state rather than direct evidence of phenotypic resistance.

Taken together, these data provide a descriptive, hypothesis-generating reference for organ-specific microbial and functional organization in the crested ibis. As such, they offer a practical framework for future captive–wild comparisons, longitudinal monitoring, and targeted validation of microbial, functional, and resistance-associated signals in conservation and health assessment.

Abbreviations

HPA, hypothalamic–pituitary–adrenal; SAM, sympathetic–adrenomedullary; SI, small intestine; AMR, antimicrobial resistance; ARG(s), antibiotic resistance gene(s); CARD, Comprehensive Antibiotic Resistance Database; EF-Tu, elongation factor Tu; GO, Gene Ontology; HMM, hidden Markov model; HUMAnN, HMP Unified Metabolic Analysis Network; KEGG, Kyoto Encyclopedia of Genes and Genomes; MetaCyc, Metabolic Pathway Database (BioCyc); MGE(s), mobile genetic element(s); MLS, macrolide–lincosamide–streptogramin; RGI, Resistance Gene Identifier; RPM, reads per million (normalized to non-host, non-rRNA reads); SCFA(s), short-chain fatty acid(s).

Availability of Data and Materials

Raw metatranscriptome sequencing reads (jejunum/duodenum, liver, spleen, and lung) have been archived in the Genome Sequence Archive (GSA) at CNCB/NGDC under BioProject PRJCA047134. The other datasets used or analyzed during the current study are available from the corresponding authors on reasonable request.

Author Contributions

GQ, JR, JS, and YX designed the study and drafted the initial manuscript. JR, JS, JJ, PZ, XW, XC, CL performed the experiments and analyzed the data. LY, WD performed sample collection and data processing. YX re-

vised the manuscript. All authors contributed to editorial changes in the manuscript. All authors read and approved the final manuscript. All authors have participated sufficiently in the work and agreed to be accountable for all aspects of the work.

Ethics Approval and Consent to Participate

Not applicable. The crested ibis (*Nipponia nippon*) is an endangered species protected under the Wildlife Protection Law of the People's Republic of China and is listed under CITES (the Convention on International Trade in Endangered Species of Wild Fauna and Flora). All research and management activities involving crested ibises are conducted in strict accordance with the Wildlife Protection Law, with proper institutional authorization from the relevant conservation authority. The tissue samples used in this study were obtained from deceased crested ibises provided by the Zhejiang Provincial Crested Ibis Rescue and Conservation Center. With permission from the Zhejiang Provincial Crested Ibis Rescue and Conservation Center, qualified personnel from the Animal Hospital of Zhejiang University performed post-mortem necropsies and tissue sampling after the animals died suddenly following an acute stress event. These animals were not euthanized, sacrificed, or subjected to any experimental procedures for this study. As this study did not involve live-animal experiments or any form of intervention on living animals, no application for formal institutional animal ethics approval was submitted in accordance with the applicable institutional policies.

Acknowledgment

We thank Christopher Wood (College of Life Sciences, Zhejiang University) for helpful discussions and English editing. We are grateful to Jiusheng Wu, Yilei Zheng, and Wenjing Chen (Zhejiang University Veterinary Teaching Hospital) for clinical guidance and discussions.

Funding

This work was supported by the Deqing County Ecological Forestry Comprehensive Service Center (Project ZJXRDQ-2024-JC64).

Conflicts of Interest

The authors declare no conflicts of interest. Given their roles as the Editorial Board members, Chen Li and Yongmei Xi had no involvement in the peer-review of this article and have no access to information regarding its peer review. Full responsibility for the editorial process for this article was delegated to Graham Pawelec.

Declaration of AI and AI-Assisted Technologies in the Writing Process

During the preparation of this work, the authors used ChatGPT-5 to check spelling and grammar. After using this tool, the authors reviewed and edited the content as needed and take full responsibility for the content of the publication.

Supplementary Material

Supplementary material associated with this article can be found, in the online version, at https://doi.org/10.31083/FBL53784.

References

[1] Okahisa Y, Nagata H. Evaluation of ongoing Crested Ibis (Nipponia nippon) reintroduction using an integrated population model and Bayesian population viability analysis. Ibis. 2022; 164: 1104–1122. https://doi.org/10.1111/ibi.13071

[2] Ma L, Li X, Zhai T, Zhang Y, Song K, Holyoak M, et al. Changes in the Habitat Preference of Crested Ibis (*Nipponia nippon*) during a Period of Rapid Population Increase. Animals: an Open Access Journal from MDPI. 2021; 11: 2626. https://doi.org/10.3390/ani11092626

[3] Zheng D, Liwinski T, Elinav E. Interaction between microbiota and immunity in health and disease. Cell Research. 2020; 30: 492–506. https://doi.org/10.1038/s41422-020-0332-7

[4] Belkaid Y, Hand TW. Role of the microbiota in immunity and inflammation. Cell. 2014; 157: 121–141. https://doi.org/10.1016/j.cell.2014.03.011

[5] Margolis KG, Cryan JF, Mayer EA. The Microbiota-Gut-Brain Axis: From Motility to Mood. Gastroenterology. 2021; 160: 1486–1501. https://doi.org/10.1053/j.gastro.2020.10.066

[6] Romero LM. Physiological stress in ecology: lessons from biomedical research. Trends in Ecology & Evolution. 2004; 19: 249–255. https://doi.org/10.1016/j.tree.2004.03.008

[7] Deviche P, Bittner S, Gao S, Valle S. Roles and Mechanistic Bases of Glucocorticoid Regulation of Avian Reproduction. Integrative and Comparative Biology. 2017; 57: 1184–1193. https://doi.org/10.1093/icb/icx112

[8] Perry SF, Capaldo A. The autonomic nervous system and chromaffin tissue: neuroendocrine regulation of catecholamine secretion in non-mammalian vertebrates. Autonomic Neuroscience: Basic & Clinical. 2011; 165: 54–66. https://doi.org/10.1016/j.autneu.2010.04.006

[9] McEwen BS, Wingfield JC. The concept of allostasis in biology and biomedicine. Hormones and Behavior. 2003; 43: 2–15. https://doi.org/10.1016/s0018-506x(02)00024-7

[10] Sapolsky RM, Romero LM, Munck AU. How do glucocorticoids influence stress responses? Integrating permissive, suppressive, stimulatory, and preparative actions. Endocrine Reviews. 2000; 21: 55–89. https://doi.org/10.1210/edrv.21.1.0389

[11] Dalile B, Van Oudenhove L, Vervliet B, Verbeke K. The role of short-chain fatty acids in microbiota-gut-brain communication. Nature Reviews. Gastroenterology & Hepatology. 2019; 16: 461–478. https://doi.org/10.1038/s41575-019-0157-3

[12] Bonaz B, Bazin T, Pellissier S. The Vagus Nerve at the Interface of the Microbiota-Gut-Brain Axis. Frontiers in Neuroscience. 2018; 12: 49. https://doi.org/10.3389/fnins.2018.00049

[13] Wahlström A, Sayin SI, Marschall HU, Bäckhed F. Intestinal Crosstalk between Bile Acids and Microbiota and Its Impact on Host Metabolism. Cell Metabolism. 2016; 24: 41–50. https://doi.org/10.1016/j.cmet.2016.05.005

[14] Turnbull AV, Rivier CL. Regulation of the hypothalamic-pituitary-adrenal axis by cytokines: actions and mechanisms of action. Physiological Reviews. 1999; 79: 1–71. https://doi.org/10.1152/physrev.1999.79.1.1

[15] Rivier C, Chizzonite R, Vale W. In the mouse, the activation of the hypothalamic-pituitary-adrenal axis by a lipopolysac-

charide (endotoxin) is mediated through interleukin-1. Endocrinology. 1989; 125: 2800–2805. https://doi.org/10.1210/endo-125-6-2800

[16] Davis AK, Maney DL, Maerz JC. The use of leukocyte profiles to measure stress in vertebrates: a review for ecologists. Functional Ecology. 2008; 22: 760–772. https://doi.org/10.1111/j.1365-2435.2008.01467.x

[17] Bortolotti GR, Marchant TA, Blas J, German T. Corticosterone in feathers is a long-term, integrated measure of avian stress physiology. Functional Ecology. 2008; 22: 494–500. https://doi.org/10.1111/j.1365-2435.2008.01387.x

[18] Goymann W. Noninvasive monitoring of hormones in bird droppings: physiological validation, sampling, extraction, sex differences, and the influence of diet on hormone metabolite levels. Annals of the New York Academy of Sciences. 2005; 1046: 35–53. https://doi.org/10.1196/annals.1343.005

[19] Shang Y, Kumar S, Oakley B, Kim WK. Chicken Gut Microbiota: Importance and Detection Technology. Frontiers in Veterinary Science. 2018; 5: 254. https://doi.org/10.3389/fvets.2018.00254

[20] Jia H, Dong N. Effects of bile acid metabolism on intestinal health of livestock and poultry. Journal of Animal Physiology and Animal Nutrition. 2024; 108: 1258–1269. https://doi.org/10.1111/jpn.13969

[21] Agus A, Planchais J, Sokol H. Gut Microbiota Regulation of Tryptophan Metabolism in Health and Disease. Cell Host & Microbe. 2018; 23: 716–724. https://doi.org/10.1016/j.chom.2018.05.003

[22] Zelante T, Iannitti RG, Cunha C, De Luca A, Giovannini G, Pieraccini G, et al. Tryptophan catabolites from microbiota engage aryl hydrocarbon receptor and balance mucosal reactivity via interleukin-22. Immunity. 2013; 39: 372–385. https://doi.org/10.1016/j.immuni.2013.08.003

[23] Franzosa EA, Morgan XC, Segata N, Waldron L, Reyes J, Earl AM, et al. Relating the metatranscriptome and metagenome of the human gut. Proceedings of the National Academy of Sciences of the United States of America. 2014; 111: E2329–E2338. https://doi.org/10.1073/pnas.1319284111

[24] Clayton JB, Vangay P, Huang H, Ward T, Hillmann BM, Al-Ghalith GA, et al. Captivity humanizes the primate microbiome. Proceedings of the National Academy of Sciences of the United States of America. 2016; 113: 10376–10381. https://doi.org/10.1073/pnas.1521835113

[25] Florkowski MR, Hamer SA, Yorzinski JL. Brief exposure to captivity in a songbird is associated with reduced diversity and altered composition of the gut microbiome. FEMS Microbiology Ecology. 2023; 99: fiad096. https://doi.org/10.1093/femsec/fiad096

[26] San Juan PA, Castro I, Dhami MK. Captivity reduces diversity and shifts composition of the Brown Kiwi microbiome. Animal Microbiome. 2021; 3: 48. https://doi.org/10.1186/s42523-021-00109-0

[27] McKenzie VJ, Song SJ, Delsuc F, Prest TL, Oliverio AM, Korpita TM, et al. The Effects of Captivity on the Mammalian Gut Microbiome. Integrative and Comparative Biology. 2017; 57: 690–704. https://doi.org/10.1093/icb/icx090

[28] Alberdi A, Martin Bideguren G, Aizpurua O. Diversity and compositional changes in the gut microbiota of wild and captive vertebrates: a meta-analysis. Scientific Reports. 2021; 11: 22660. https://doi.org/10.1038/s41598-021-02015-6

[29] Parada Venegas D, De la Fuente MK, Landskron G, González MJ, Quera R, Dijkstra G, et al. Short Chain Fatty Acids (SCFAs)-Mediated Gut Epithelial and Immune Regulation and Its Relevance for Inflammatory Bowel Diseases. Frontiers in Immunology. 2019; 10: 277. https://doi.org/10.3389/fimmu.2019.00277

[30] Guzior DV, Quinn RA. Review: microbial transformations of human bile acids. Microbiome. 2021; 9: 140. https://doi.org/10.1186/s40168-021-01101-1

[31] Douterelo I, Sharpe RL, Husband S, Fish KE, Boxall JB. Understanding microbial ecology to improve management of drinking water distribution systems. Wiley Interdisciplinary Reviews: Water. 2019; 6: e1325. https://doi.org/10.1002/wat2.1325

[32] Jia T, Chang WS, Marcelino VR, Zhao S, Liu X, You Y, et al. Characterization of the Gut Microbiome and Resistomes of Wild and Zoo-Captive Macaques. Frontiers in Veterinary Science. 2021; 8: 778556. https://doi.org/10.3389/fvets.2021.778556

[33] Pal C, Bengtsson-Palme J, Kristiansson E, Larsson DGJ. Co-occurrence of resistance genes to antibiotics, biocides and metals reveals novel insights into their co-selection potential. BMC Genomics. 2015; 16: 964. https://doi.org/10.1186/s12864-015-2153-5

[34] Michaelis C, Grohmann E. Horizontal Gene Transfer of Antibiotic Resistance Genes in Biofilms. Antibiotics (Basel, Switzerland). 2023; 12: 328. https://doi.org/10.3390/antibiotics12020328

[35] Ojala T, Häkkinen AE, Kankuri E, Kankainen M. Current concepts, advances, and challenges in deciphering the human microbiota with metatranscriptomics. Trends in Genetics: TIG. 2023; 39: 686–702. https://doi.org/10.1016/j.tig.2023.05.004

[36] Westermann AJ, Barquist L, Vogel J. Resolving host-pathogen interactions by dual RNA-seq. PLoS Pathogens. 2017; 13: e1006033. https://doi.org/10.1371/journal.ppat.1006033

[37] Mika-Gospodorz B, Giengkam S, Westermann AJ, Wongsantichon J, Kion-Crosby W, Chuenklin S, et al. Dual RNA-seq of Orientia tsutsugamushi informs on host-pathogen interactions for this neglected intracellular human pathogen. Nature Communications. 2020; 11: 3363. https://doi.org/10.1038/s41467-020-17094-8

[38] Qi X, Zhang Y, Zhang Y, Luo F, Song K, Wang G, et al. Vitamin B_{12} produced by Cetobacterium somerae improves host resistance against pathogen infection through strengthening the interactions within gut microbiota. Microbiome. 2023; 11: 135. https://doi.org/10.1186/s40168-023-01574-2

[39] Wang A, Zhang Z, Ding Q, Yang Y, Bindelle J, Ran C, et al. Intestinal *Cetobacterium* and acetate modify glucose homeostasis via parasympathetic activation in zebrafish. Gut Microbes. 2021; 13: 1–15. https://doi.org/10.1080/19490976.2021.1900996

[40] Prescott JF, Parreira VR, Mehdizadeh Gohari I, Lepp D, Gong J. The pathogenesis of necrotic enteritis in chickens: what we know and what we need to know: a review. Avian Pathology. 2016; 45: 288–294. https://doi.org/10.1080/03079457.2016.1139688

[41] Qiu G, Ran J, Shi J, Liu X, Chen Y, Yuan L, et al. Environmental Triggers and Behavioral, Imaging and Pathological Correlates of Stress-induced Sudden Death in the Crested Ibis. Chinese Journal of Wildlife. 2026; 47: 86–99. https://doi.org/10.12375/ysdwxb.202509005

[42] Sun F, Chen J, Liu K, Tang M, Yang Y. The avian gut microbiota: Diversity, influencing factors, and future directions. Frontiers in Microbiology. 2022; 13: 934272. https://doi.org/10.3389/fmicb.2022.934272